Extracting horizons and sequence boundaries from 3D seismic images

Xinming Wu & Dave Hale
Center for Wave Phenomena, Colorado School of Mines, Golden, CO 80401, USA

SUMMARY

Automated horizon-extraction methods often have difficulty extracting horizons that terminate at unconformities or sequence boundaries. Using sequence boundaries as constraints is one way to solve this problem, but there exists no automated method for sequence-boundary extraction. We first introduce a globally optimal method to efficiently extract a horizon from a seismic image. We then use scattered control points as constraints to enable our horizon-extraction method to extract sequence boundaries. Finally, we propose an active-surface method to refine extracted horizons to align them with amplitude peaks or troughs and thereby reveal more geologic details.

INTRODUCTION

Horizons and sequence boundaries are geologically significant surfaces that can be extracted from seismic images. Horizons refer to those seismic reflectors representing stratal surfaces of constant geologic time. Sequence boundaries coinciding with unconformities can also be extracted along reflectors, but they represent geologically time-variable surfaces (Vail et al., 1977).

Both locally and globally optimal methods have been developed to automatically extract horizons. Locally optimal methods extract horizons by searching the peaks or troughs of seismic reflectors. Horizons extracted using these methods can follow small-scale geologic structures and thus they are helpful for revealing geologic details. These methods, however, are usually sensitive to noise and limited to simple geology (Hoyes and Cheret, 2011). Globally optimal methods (e.g., Lomask et al., 2006; Parks et al., 2010; Luo and Hale, 2012; Stark, 2005; Wu and Zhong, 2012a,b) flatten an entire 3D seismic image and obtain all globally optimized horizons in the seismic image simultaneously. They are more robust for noisy data, however, horizons extracted using these methods are usually smooth and therefore lack detailed geologic structures.

In addition, all of the horizon-extraction methods discussed above share the common difficulty in extracting horizons that terminate at an unconformity or sequence boundary. One way to solve this problem is to first extract all sequence boundaries in a seismic image and then use them as constraints while extracting other horizons. However, no method has yet been developed to extract sequence boundaries automatically.

In this paper, we first introduce a horizon-extraction method that uses seismic normal vectors to efficiently extract a globally optimized horizon from a seismic image. We then discuss the use of sparse control points that constrain our horizon-extraction method to extract sequence boundaries. Finally, we introduce an *active-surface method* that uses seismic amplitudes to refine horizons to resolve more geologic detail.

HORIZON EXTRACTION

We first use structure tensors (van Vliet and Verbeek, 1995; Fehmers and Höcker, 2003) to compute seismic normal vectors $\mathbf{n} = [n_x \; n_y \; n_z]^T$ that are locally perpendicular to seismic reflectors. We then assume a surface $z = f(x,y)$ that is initially horizontal at some specified depth or time. The normal vectors of the surface can be computed as

$$\mathbf{n}_s = \alpha[-f_x \;\; -f_y \;\; 1]^T \tag{1}$$

where $f_x \equiv \partial f(x,y)/\partial x$, $f_y \equiv \partial f(x,y)/\partial y$, and α is a scale factor to normalize $\mathbf{n}_s$ as unit vectors. To extract a seismic horizon, we seek to find a surface whose normal vectors $\mathbf{n}_s$ equal the seismic normal vectors $\mathbf{n}$ at corresponding points in the 3D seismic image:

$$\alpha[-f_x \;\; -f_y \;\; 1]^T = [n_x \;\; n_y \;\; n_z]^T. \tag{2}$$

Therefore, setting $\alpha = n_z$, we solve the following inverse gradient problem to extract the horizon surface $z = f(x,y)$,

$$\alpha[f_x \;\; f_y]^T = [p \;\; q]^T. \tag{3}$$

where $p = -n_x/n_z$ and $q = -n_y/n_z$ are reflector slopes in the x and y directions, respectively. Similar to Wei and Klette (2002), we solve this problem by minimizing

$$\begin{aligned} E = &\int\int_\Omega \frac{1}{2}(|f_x - p|^2 + |f_y - q|^2)dxdy \\ &+ \frac{\mu}{2}\int\int_\Omega (|f_{xx}|^2 + 2|f_{xy}|^2 + |f_{yy}|^2)dxdy. \end{aligned} \tag{4}$$

The second term is related to surface curvatures and is used to improve the robustness of the method for noisy or chaotic seismic reflectors. The value $\mu \geq 0$ weights this surface-curvature term. To minimize the above cost function E, we use the calculus of variations to obtain the Euler-Lagrange equation:

$$\triangle f - \mu \triangle^2 f = \nabla \cdot \mathbf{g}, \tag{5}$$

where $\mathbf{g} = [p \; q]^T$, $\triangle f = f_{xx} + f_{yy}$, and $\triangle^2 f = f_{xxxx} + 2f_{xxyy} + f_{yyyy}$. By solving this equation, we can update the surface $z = f(x,y)$ so that its normal vectors $\mathbf{n}_s$ match the seismic normal vectors $\mathbf{n}$ at all points $(x,y,z = f(x,y))$ on the surface.

In Figure 1, using only one control point to indicate the sequence boundary we want to extract, our method updates the initially horizontal surface to the more nearly correct position (blue curves in Figure 1) after 9 iterations. The updated surface is well aligned with reflectors in the conformable areas (left section in Figure 1a) where normal vectors can be estimated accurately. However, the surface is not updated to the correct location at the angular unconformity (green dashed curve in Figure 1b). Automatically extracting such a sequence boundary or unconformity is an important but difficult problem. Using structure tensors, we fail to estimate correct normal vectors at an angular unconformity, but instead compute smoothed

DOI http://dx.doi.org/10.1190/segam2013-0296.1

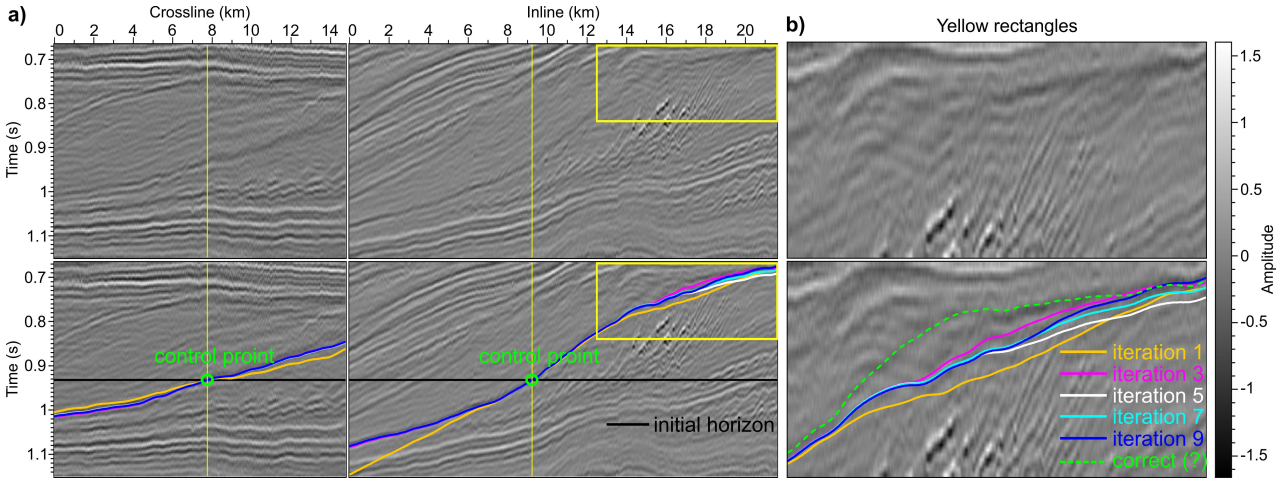

Figure 1: Seismic sections (a) and subsections (b) that intersect with a sequence boundary. The initially horizontal surface (black curve) passes through one control point and is updated iteratively using seismic normal vectors. The dashed green curve denotes the sequence boundary extracted using 26 control points.

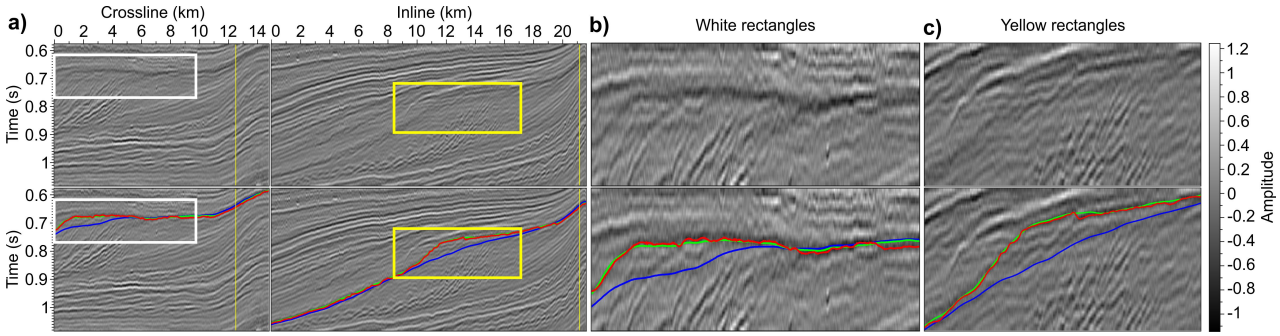

Figure 2: Seismic sections (a) and subsections (b) and (c) that intersect with an extracted sequence boundary using one control point (blue curve), 26 control points (green curve), and after refining (red curve) using our active-surface method.

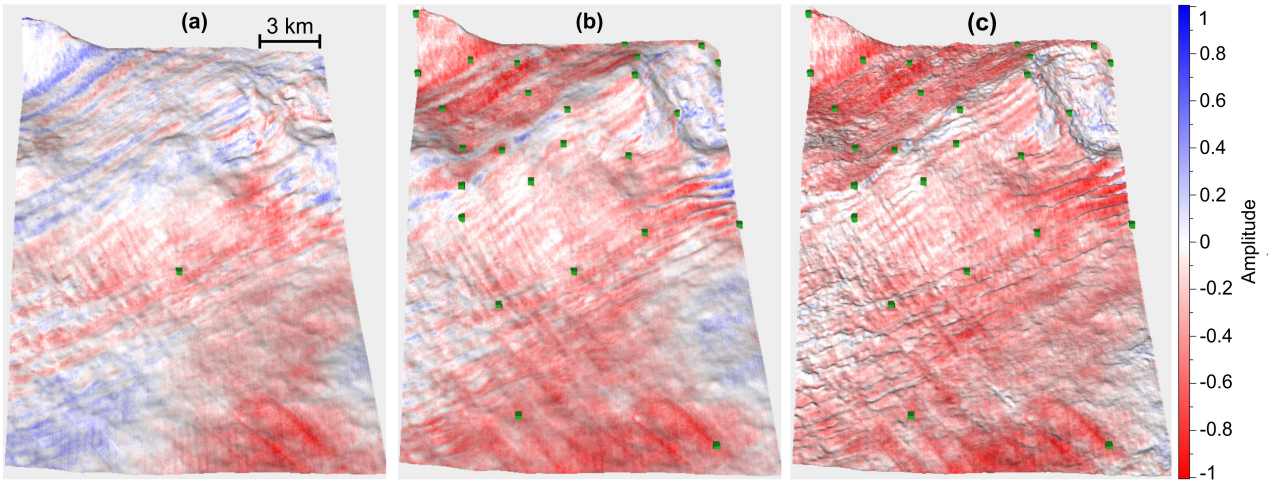

Figure 3: A 3D view of the amplitude-colored sequence boundaries (blue, green and red curves in Figure 2) that are extracted using (a) one control point, (b) 26 control points, and (c) 26 control points with refinement using our active-surface method. The green points are control points.

DOI http://dx.doi.org/10.1190/segam2013-0296.1

vectors that yields the incorrect surface in angular unconformity areas. In the next section, we describe how to correctly extract a sequence boundary using sparse control points.

SEQUENCE BOUNDARY EXTRACTION

Near unconformities or in areas where the image is noisy, the estimated normal vector field is not reliable enough to extract a correct sequence boundary or horizon. In such cases, we use a small number of scattered control points $(x_i, y_i, z_i), i = 1, \ldots, n$ to interpolate a correction that updates the surface described the above section to extract an accurate sequence boundary or horizon in a noisy image. In each iteration of surface updating, we first compute an updated surface $z = f(x,y)$ using seismic normal vectors. Similar to Horovitz and Kiryati (2004), we then use the thin-plate spline interpolation method to interpolate a correction $z_c = c(x,y)$ by using the depth differences $z_i - f(x_i, y_i)$ between the control points and the updated surface. The surface is then corrected using the interpolated correction field, before the next iteration.

Thin-plate spline interpolation

Thin-plate spline interpolation is a classic method for interpolation of scattered data to yield a smooth function $c(x,y)$ that minimizes the integral

$$I(c) = \int\int_{\Omega} (|c_{xx}|^2 + 2|c_{xy}|^2 + |c_{yy}|^2) dxdy, \tag{6}$$

while satisfying the interpolation conditions

$$c(x_i, y_i) = z_i, \; i = 1, 2, \ldots, n. \tag{7}$$

Duchon (1977) shows that the interpolating function $c(x,y)$ has the form

$$c(x,y) = a_0 + a_1 x + a_2 y + \sum_{i=1}^{n} w_i \phi(r_i), \tag{8}$$

where r_i is the distance between the i-th control point (x_i, y_i) and $(x,y) \in \Omega$, a_0, a_1 and a_2 are coefficients, and $\phi(r) = r^2 log(r)$, $0 < r < \infty$. The coefficients w_i satisfy

$$\sum_{i=1}^{n} w_i = 0, \; \sum_{i=1}^{n} w_i x_i = 0, \; \sum_{i=1}^{n} w_i y_i = 0. \tag{9}$$

From the correction values known at the control points,

$$c(x_i, y_i) = z_i - f(x_i, y_i), \tag{10}$$

we can compute the coefficients $[w_1 \; \cdots \; w_n \; a_0 \, a_1 \, a_2]$, and then use equation 8 to interpolate correction values $c(x,y)$ at every (x,y) for which the surface is defined. The horizon $f(x,y)$ updated by using seismic normal vectors is then corrected by

$$f_c(x,y) = f(x,y) + c(x,y). \tag{11}$$

This corrected horizon $f_c(x,y)$, which now honors the control points, is then used for the next iteration.

Results using control points

The sequence boundary extracted (green curves in Figures 1 and 2) with 26 control points correctly follows the unconformity while the one (blue curves in Figures 1 and 2) with one control point fails. In the 3-D view of amplitude-colored sequence boundaries, amplitude values for 26 control points (Figure 3b) are more uniform than for one control point (Figure 3a). Moreover, the initial surface takes 9 iterations to converge using one control point but only 5 iterations using 26 control points. The extracted sequence boundary with 26 control points is further refined (Figure 3c and red curves in Figure 2) by using the active-surface method which we discuss in the next section.

SURFACE REFINEMENT

Using the global optimization and orientations estimated from locally averaged structures, horizon-extraction methods might smooth out some subtle geologic structures or details that can be important in geologic interpretations. To reveal more subtle geologic structures in a horizon, we propose an active-surface method to refine extracted horizons.

Active surface

The active-snake or active-contour model, first introduced by Kass et al. (1988), is a powerful method for detecting closed boundary curves in 2D image segmentations. The active-snake method is based on energy-minimizing spline curves influenced by internal forces and external image forces. The external image forces pull an initial contour to nearby edges in the 2D image, while the internal forces preserve the original shape and smoothness of the contour. Chopra and Marfurt (2008) suggest that the active-snake or active-contour method might be used to detect channels and other stratigraphic features. In this paper, we discuss an active surface that is an open surface that deforms vertically to align with nearby peaks or troughs in seismic amplitude.

A globally optimized horizon $z = f(x,y)$ that is consistent with reflector structure is not necessarily aligned with seismic peaks or troughs. We take the horizon as an active surface, and define the energy of the active surface using an internal energy term E_{int} and an external energy term E_{ext}. The internal energy of the active surface is defined by using the surface curvature approximation used in equations 4 and 6:

$$E_{int}(f) = \int\int_{\Omega} \frac{1}{2} (|f_{xx}|^2 + 2|f_{xy}|^2 + |f_{yy}|^2) dxdy, \tag{12}$$

the external energy is related to seismic amplitudes $A(x,y,z)$:

$$E_{ext}(f) = \int\int_{\Omega} \pm A(x, y, f(x,y)) dudv. \tag{13}$$

To align the horizon with seismic troughs we simply use the amplitude $A(x,y,f(x,y))$; to align with seismic peaks we use $-A(x,y,f(x,y))$. Assume we want the horizon to be aligned with troughs. Then the total energy of the active surface is

$$E(f) = \int\int_{\Omega} [\frac{\beta}{2} (|f_{xx}|^2 + 2|f_{xy}|^2 + |f_{yy}|^2) + A(x,y,f(x,y))] dxdy. \tag{14}$$

Again using the calculus of variations, we derive the following Euler-Lagrange equation to minimize the above energy func-

DOI http://dx.doi.org/10.1190/segam2013-0296.1

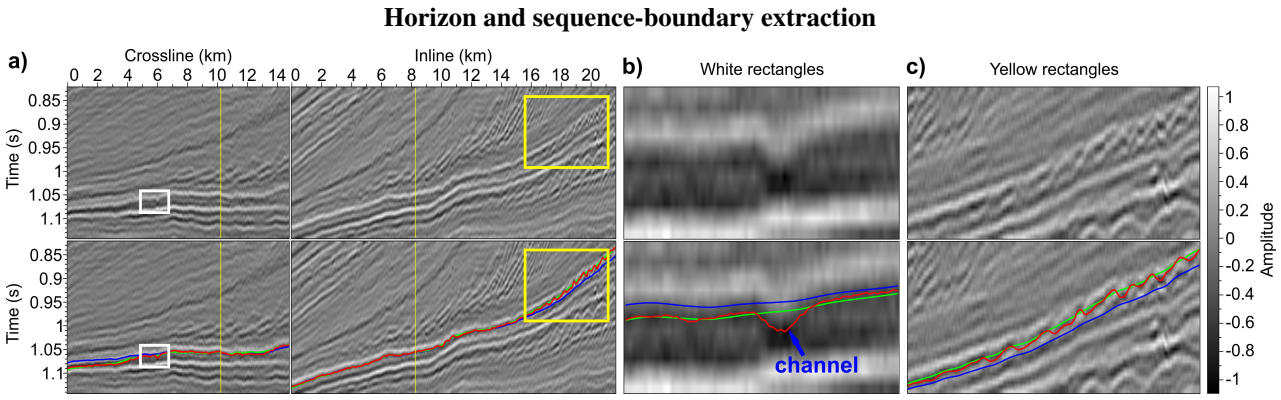

Figure 4: Seismic sections (a) and subsections (b) and (c) that intersect with an extracted seismic horizon using one control point (blue curve), 25 control points (green curve), and after refining (red curve) using our active-surface method.

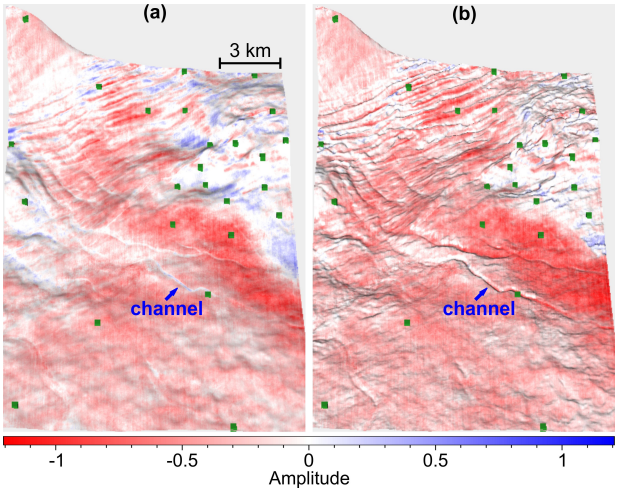

Figure 5: A 3D view of the amplitude-colored horizons (green and red curves in Figure 4) that are extracted with (a) 25 control points (green points) and (b) after refinement.

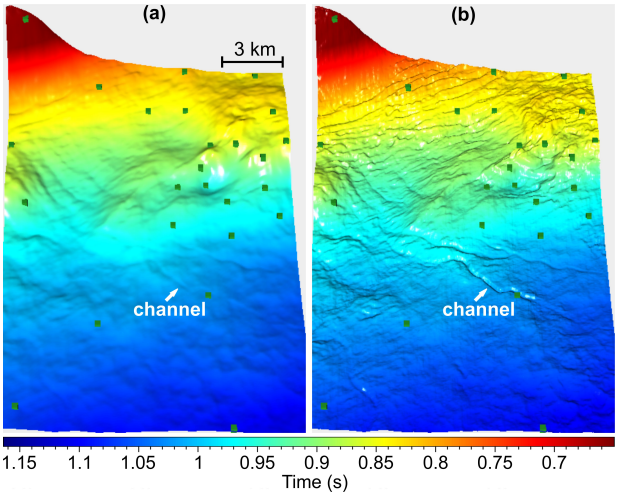

Figure 6: A 3D view of the time-colored horizons (green and red curves in Figure 4) that are extracted with (a) 25 control points (green points) and (b) after refinement.

tion and to align the horizon $z = f(x,y)$ with nearby seismic troughs:

$$\beta \triangle^2 f + \frac{\partial A}{\partial z}|_{z=f(x,y)} = 0. \quad (15)$$

Results for the active-surface method

The globally optimized horizons extracted with (blue curves in Figure 4) one control point and with (Figures 5a and 6a and green curves in Figure 4) 25 control points are smooth. Applying our active-surface method to the horizons (green curves in Figures 2 and 4), we obtain refined horizons (red curves in Figures 2 and 4) that are well aligned with seismic troughs. In the 3D views of the refined horizons (Figures 3c, 5b and 6b), we see many subtle geologic structures that cannot be seen in the unrefined horizons. For example, although we observe some amplitude variations that indicate the existence of a channel in the globally optimized horizon (Figure 5a), the incised valley structure of the channel is not apparent. After refinement, we clearly see the cross-section of the incised channel in Figure 4b. The incised valley structure and shape of the channel are readily and continuously apparent in both the amplitude- (Figure 5b) and time-colored (Figure 6b) horizons.

CONCLUSION

Our horizon-extraction method extracts any horizon we choose in a seismic image by using one control point that indicates the chosen horizon. When we sparsely define control points at angular unconformities, the horizon-extraction method can be improved to extract sequence boundaries. Of course, we can also choose control points in complicated areas with noise or chaotic reflectors to extract more reliable horizons in such areas. Using the active-surface method, extracted horizons can be well aligned with seismic peaks or troughs to reveal more geologic detail.

ACKNOWLEDGMENTS

This research is supported by the sponsor companies of the Consortium Project on Seismic Inverse Methods for Complex Structures. The seismic images shown in this paper were provided by dGB Earth Sciences.

DOI http://dx.doi.org/10.1190/segam2013-0296.1

http://dx.doi.org/10.1190/segam2013-0296.1

EDITED REFERENCES

Note: This reference list is a copy-edited version of the reference list submitted by the author. Reference lists for the 2013 SEG Technical Program Expanded Abstracts have been copy edited so that references provided with the online metadata for each paper will achieve a high degree of linking to cited sources that appear on the Web.

REFERENCES

Chopra, S., and K. J. Marfurt, 2008, Emerging and future trends in seismic attributes: The Leading Edge, **27**, 298–318, http://dx.doi.org/10.1190/1.2896620.

Duchon, J., 1977, Splines minimizing rotation-invariant seminorms in Sobolev spaces, *in* W. Shemp and K. Zeller, eds., Construction theory of functions of several variables: Springer, 85–100.

Fehmers, G. C., and C. Höcker, 2003, Fast structural interpretation with structure-oriented filtering: Geophysics, **68**, 1286–1293, http://dx.doi.org/10.1190/1.1598121.

Horovitz, I., and N. Kiryati, 2004, Depth from gradient fields and control points: Bias correction in photometric stereo: Image and Vision Computing, **22**, 681–694, http://dx.doi.org/10.1016/j.imavis.2004.01.005.

Hoyes, J., and T. Cheret, 2011, A review of "global" interpretation methods for automated 3D horizon picking: The Leading Edge, **30**, 38–47, http://dx.doi.org/10.1190/1.3535431.

Kass, M., A. Witkin, and D. Terzopoulos, 1988, Snakes: Active contour models: International Journal of Computer Vision, **1**, no. 4, 321–331, http://dx.doi.org/10.1007/BF00133570.

Lomask, J., A. Guitton, S. Fomel, J. Claerbout, and A. A. Valenciano, 2006, Flattening without picking: Geophysics, **71**, no. 4, P13–P20, http://dx.doi.org/10.1190/1.2210848.

Luo, S., and D. Hale, 2012, Unfaulting and unfolding 3D seismic images: Colorado School of Mines Center for Wave Phenomena (CWP) Report 722.

Parks, D., 2010, Seismic image flattening as a linear inverse problem: M.S. thesis, Colorado School of Mines.

Stark, T. J., 2005, Generating a seismic Wheeler volume: 75th Annual International Meeting, SEG, Expanded Abstracts, 782–785.

Vail, P. R., R. G. Todd, and J. B. Sangree, 1977, Seismic stratigraphy and global changes of sea level: Part 5. Chronostratigraphic significance of seismic reflections, *in* C. E. Payton, ed., Seismic stratigraphy — Applications to hydrocarbon exploration: AAPG Memoir 26, 99–116.

van Vliet, L. J., and P. W. Verbeek, 1995, Estimators for orientation and anisotropy in digitized images: Proceedings of the 1st Annual Conference of the Advanced School for Computing and Imaging (ASCI), 442–450.

Wei, T., and R. Klette, 2002, Height from gradient using surface curvature and area constraints: 3rd Indian Conference on Computer Vision, Graphics and Image Processing, 204–210.

Wu, X., and G. Zhong, 2012a, Generating a relative geologic time volume by 3D graph-cut phase unwrapping method with horizon and unconformity constraints: Geophysics, **77**, no. 4, O21–O34, http://dx.doi.org/10.1190/geo2011-0351.1.

DOI http://dx.doi.org/10.1190/segam2013-0296.1

Wu, X., and G. Zhong, 2012b, A method for generating a seismic Wheeler volume via a relative geologic time volume: 82nd Annual International Meeting, SEG, Expanded Abstracts, doi:10.1190/segam2012-1177.1.

DOI http://dx.doi.org/10.1190/segam2013-0296.1